DIMACS Technical Report 99-27
5/29/99

Efficient Radio Wave Front Propagation for Wireless Radio Signal Prediction[1]

by

Greg Perkins
gperkins@paul.rutgers.edu

Diane Souvaine
dls@cs.rutgers.edu

Department of Computer Science, Rutgers University, Piscataway, NJ 08855

[1]Research supported in part by DIMACS NSF Grant #NCR-9527163. Diane Souvaine's current address is: EECS dept., Tufts University, Medford, MA 02155, dls@eecs.tufts.edu

DIMACS is a partnership of Rutgers University, Princeton University, AT&T Labs-Research, Bell Labs, Telcordia Technologies (formerly Bellcore) and NEC Research Institute.

DIMACS is an NSF Science and Technology Center, funded under contract STC–91–19999; and also receives support from the New Jersey Commission on Science and Technology.

ABSTRACT

Due to the ever increasing complexity of wireless network design, wireless network simulation engines have become a necessary tool for wireless network engineers. A signal-strength prediction system lies at the foundation of every wireless simulator, making signal-strength prediction for microcells and picocells an important research topic in the radio field. Efficient and accurate methods are needed for use in current wireless network design and future wireless network research.

This paper describes a system, PREDICT, designed for use in wireless radio signal prediction research. PREDICT tracks the expansion of a transmitter's wavefront by modeling the wavefront as an ever expanding sphere centered upon the transmitter. The sphere's expansion is tracked by discretizing the sphere's surface with a triangulation and then propagating each triangular wavefront through the environment. In the propagation prediction of these triangular wave fronts, PREDICT supports reflection, transmission and diffraction based upon the geometric optics (GO) model of electromagnetic waves. Signal prediction is performed through a special summation of the predicted multi-path at a receiver.

PREDICT's algorithms have been specifically designed for use in radio signal prediction. The current environments supported by PREDICT are urban with flat or varied terrain and a single floor of a building, where all obstacles in the environment have vertical or horizontal walls. The system design is flexible, allowing PREDICT to be expanded for use in many different environments. Modularity allows for easy modification to the GO model or implementation of alternate radio modeling methods (one can easily modify PREDICT, or use the results generated by PREDICT, with one's own radio wave modeling methods). Preliminary testing has been completed. After more extensive testing PREDICT will be publicly available for any non-commercial use.

1 Introduction

Wireless network design and system implementation are two large and growing research areas due to the ever increasing demand for wireless communications. Given a narrow band of frequencies to work with, wireless network engineers are faced with the problem of providing good, clear reception to many users. Many issues arise during the solution to this problem, a few of the larger ones are transmitter placement, signal interference and frequency allocation (in both fixed and dynamic selection strategies). Some more specific issues are deciding which algorithms to implement for the various demands of a wireless communications network: hand-off, the passing of a user from one base station to the next; user location, using the wireless system to accurately locate the position of a user; and transmitter failure, how the system handles the rerouting of users when a transmitter fails due to a power outage or mechanical failure. Since field testing is both expensive and time consuming, engineers and researchers are now turning to wireless network simulation engines for preliminary testing of their designs and new theories (in the case of transmitter placement, these systems can often find the preliminary design without human help, see Fortune, *et al* [9], [27] and SMT Plus [25]). A system for signal-strength prediction is a necessary tool for identifying appropriate solutions in each of the problems cited above.

The need for fast and accurate signal-strength prediction systems is clear. The methods for accurate macrocell[1] signal prediction, developed over twenty years ago, have proven inaccurate for microcell and picocell prediction. To date, the most versatile and accurate methods for microcell and picocell environments are based upon the geometric optics model (GO) (see [1], [9], [14], [16], [23], [17] and [27]) in which a radio signal is modeled as a ray. Using the GO model and some method for tracing rays, a radio wave signal can be simulated through the propagation of the associated ray in the user specified environment. Predicted signal strengths at query points, user-specified points at which signal prediction is desired, can be determined by combining the multiple predicted signal paths which arrive at a query point. Under this scheme reflection, transmission, scattering and diffraction can all be adequately modeled.

When using ray-tracing in signal-propagation prediction, the traced ray does not represent a single radio signal. Instead, each ray represents a portion of the radio wavefront. Most of the previously mentioned systems account for this fact by using a *capture cone*, an ever-expanding cone centered upon the ray. Query points are 'intersected' by the ray path if they lie within the capture cone. Although this is a reasonable solution, it does lead to artifacts because reflection, transmission, diffraction and scattering events are only computed when the ray, not the capture cone, intersect an obstacle (see [7]). A solution to this problem is to explicitly propagate the entire radio wavefront through the environment, rather than just the traced rays.

This paper presents a system, PREDICT, which is designed to efficiently predict the propagation of radio wavefronts without suffering from the above mentioned arti-

[1]See Section A for a review of radio field terminology

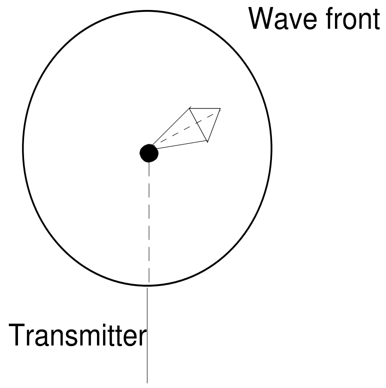

Figure 1: The spherical wavefront, as modeled by PREDICT, with an example tetra-wave

facts. The algorithms are general enough that PREDICT can be used for propagation prediction in any environment, including rough terrain, as long as obstacle walls are vertical and horizontal. It can currently be used to handle in-building prediction for a single floor, and can be extended naturally to handle any number of building floors, a planned future improvement.

PREDICT extends the notion of tracing radio signal paths by providing methods for tracing the propagation of radio wavefronts. A transmitter produces a radio wavefront where a wavefront is defined as the surface of a propagating wave that is the locus of all points having identical phase. The phase of a wave defines the wave's periodic state at time t. The wavefront is modeled by PREDICT as a one meter sphere centered upon the location of the transmitter. The wavefront is then triangulated as the triangulation of the sphere. Each triangle represents a portion of the radio wavefront (see figure 1). PREDICT then traces the path of each triangular wavefront patch as it propagates through the environment. A signal path from the transmitter to a query point is known to exist when PREDICT determines that a propagating wavefront has intersected the query point. As discussed later, the propagation path of a wave front that captures a *query point* q is topologically identical to a path of a radio signal from the transmitter to q, where a query point is a point at which signal prediction is desired. In this fashion radio signal paths are computed from the transmitter to all query points in the environment.

Only minimal validation of our propagation prediction models has been performed to date, a comparison between PREDICT and Amitay's canyon model (see Section 4). This comparison shows that PREDICT provides accurate results in the simplified setting of an ideal canyon. Further validation on real data is planned, at which time we expect good results since PREDICT's modeling assumptions are based upon the work of Fortune and Rappaport, two of the most accurate prediction systems to date ([9], [23]). This approach has allowed us to focus our efforts upon the design and construction, rather than validation, of a fast and versatile radio wave propagation prediction system, a goal we have accomplished since PREDICT is fast and able to run in parallel. As will be discussed, our implemented modeling methods have been designed to be conservative so that PREDICT returns all possible paths of interest and, consequently, makes PREDICT an optimistic signal strength prediction system. As other researchers use and provide feedback on PREDICT, we shall be able to refine our current methods and models.

Section 2 explains the modeling choices made and used in the PREDICT system, all of which are based upon the geometric optics model (GO) of radio waves (see Appendix B). Section 3 provides details on the algorithms implemented for the PREDICT system. Section 4 presents the comparison test results along with demonstrations of PREDICT in action in urban environments. Section 5 discusses related work. Section 6 provides a look into future work followed by the conclusion.

2 PREDICT and CANYON's propagation models

PREDICT's model is designed for radio wave signal prediction in both outdoor and indoor environments which adhere to the assumptions stated in Section 2.1.1 and contain microcell and/or picocell transmitters. Amitay's canyon model was designed for radio wave signal prediction in an ideal canyon, a canyon with parallel walls to infinity and whose height is higher than the transmitters.

2.1 PREDICT's propagation model

PREDICT models a radio signal wavefront as an ever expanding sphere centered upon the location of the transmitting antenna. As the sphere expands, the wavefront encounters obstacles. To track the propagation of a wavefront, PREDICT triangulates (tessellates) the sphere and then tracks the propagation of each triangular patch. A triangular patch represents an approximation to the instantaneous location of a triangular piece of the wavefront (see figure 1). A *tetra-wave* will be defined as the tetrahedral cone that is swept as a triangular patch propagates in time. When a tetra-wave intersects a query point q we will say q has been *captured*. PREDICT's model maintains the invariant that when a query point q is captured by a tetra-wave c, it must be the case that a path p exists from the transmitter to the query point q such that p is completely contained within the volume swept by the tetra-wave c (see figure 2). The model used by PREDICT tracks the reflection, transmission and diffraction of each tetra-wave. Splitting of tetra-waves is used to increase the accuracy of the prediction. Scattering and signal phase are not modeled. Specifics follow.

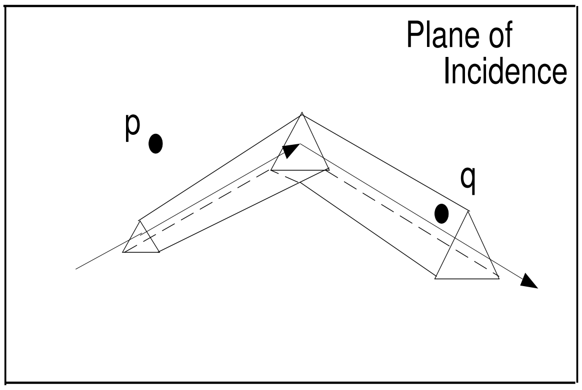

Figure 2: A tetra-wave reflecting off a wall and then capturing query point q.

2.1.1 PREDICT's environment

PREDICT's assumptions:
* all obstacle walls are either vertical or horizontal
* all obstacles are convex (no tunnels or overpasses)
* the terrain can be flat or described by a height field
* radio signals only propagate through lossless mediums
* when making outdoor predictions, signals transmitted into buildings are assumed to stay within the building the transmitted signal has passed into. Therefore, the transmitted components of radio signals are ignored in the outdoor environment.

These assumptions are reasonable for most urban or suburban settings and buildings.

2.1.2 Reflection and Transmission

When computing Γ and T, the reflected and transmitted components of a radio signal, a number of simplifying assumptions must be made. Our assumptions, outlined and defended below, determined the following Fresnel formulas 4, 5, 8 and 9 for use in computing Γ and T. The reader unfamiliar with radio theory may need to consult Appendix B.2.

Most materials have permeability values approximately equal to the free space permeability constant μ_0. Therefore, when calculating the reflection and transmission coefficients PREDICT assumes that the two mediums involved in a reflected and transmitted signal have permeability constants $\mu_1 = \mu_2 = \mu_0$. For materials like air, concrete, brick and asphalt this is a fairly reasonable assumption. Materials like steel and other good conductors do not have m values close to μ_0, but we can assume that good conductors totally reflect a radio signal and, consequently, we do not need to model the propagation of radio signals through good conductors (see Appendix B.2.3).

A radio signal's polarization is not tracked by PREDICT. In this paper we copy Seidel and Rappaport's approach in [23] which, when combined with the above as-

FREQ.	Concrete		Brick		Limestone	
MHz	ε_r	σ	ε_r	σ	ε_r	σ
		(S/m)		(S/m)		(S/m)
1723	6.11	0.133	4.62	0.0174	7.36	0.0235
2000	5.64	0.153	4.50	0.0173	7.25	0.0213
2600	5.10	0.146	4.26	0.0197	7.06	0.0179
3230			4.40	0.00324	7.13	0.0232
8200			4.45	0.0225	6.73	0.0259
12000			4.40	0.0502	29.6	0.434

Table 1: Table 1: Empirically measured dielectric and conductivity constants for concrete, brick and limestone

Material	Class	Relative Permeability μ_{sr}
Copper	Diamagnetic	0.999991
Water	Diamagnetic	0.999991
Air	Paramagnetic	1.0000004
Aluminum	Paramagnetic	1.00002
Mild Steel	Ferromagnetic	2,000
Iron	Ferromagnetic	5,000

Table 2: The Relative Static Permeabilities for Various Materials

sumption, allows us to use the perpendicular (horizontal) polarization equations (4 and 5) for vertical walls and the parallel (vertical) polarization equations (8 and 9) for ground and horizontal walls when computing Γ and T for use in the multi-path signal-strength equation 13 (see Appendix B.2.3 and B.3.2). This is a simplifying assumption which is based upon the fact that in practice radio transmitters are always vertically polarized.

This paper uses dielectric and conductivity constants provided by Sou *et al.* [26]: values for concrete, brick and limestone over the 1723 - 18000 MHz frequency range (see Table 1). The average ground dielectric constant, $\varepsilon_g = 15$, comes from [20][2]. This paper assumes that permeability values for wall materials are approximately the same as that of free space, μ_0. Example values can be found in Table 2 ([4]).

Fortunately, exact values for these constants do not appear to be critical, e.g. Seidel and Rappaport [23]. Plots of the effects of varying the dielectric values to the reflection and transmission coefficients presented in Section 2.1.6 support this claim.

[2] Note that ground dielectric values can range from 4 to 30

2.1.3 Diffraction and Scattering

PREDICT implements the universal theory of diffraction proposed by Kouyoumjian and Pathak [13] and then later extended in [19]. Code for the computation of D_s and D_h was taken directly from the text Balanis [4], pp. 848-850. Since PREDICT is designed for urban, suburban and in-building prediction with vertical and horizontal walls, PREDICT supports wedge diffraction but not tangential diffraction over curves.

It is hard to determine if diffraction is necessary for signal-strength prediction in the microcell and picocell situation. Experiments by Laurenson, *et. al* [16] showed no real benefit from the use of diffraction in their ray-tracing modeling system. This may not be surprising since the strength of a diffracted signal is directly related to the wavelength λ. The smaller the wavelength the weaker the diffracted signal. As one increases signal frequency the wavelength decreases which leads to less signal power that diffracts around corners or tangents to curved surfaces. At 950 MHz to 5 GHz, typical frequencies used in microcells and picocells, the wavelength ranges from 31.6 cm to 6 cm. One can conclude that as microcells and picocells utilize higher frequencies diffraction will become a less important phenomena.

Scattering is not modeled in the PREDICT system since scattering is hard to accurately model and does not appear to be important for average signal-strength prediction. A reason for this phenomenon may lie in the fact that even though a radio signal may be scattered the largest component of the radio signal propagates in the direction predicted by Snell's Law. Furthermore, work by Fortune *et. al* [9] and Seidel and Rappaport [23] achieved good predictive accuracy without modeling scattering effects.

2.1.4 Computing the Signal Strength for a Propagation Path p

Let path p_i represent the radio signal path from the transmitter to query point q which lies within tetra-wave c where s_i is the signal strength for p_i at the transmitter. To calculate the radio signal strength of p_i at q requires attenuation of s_i due to distance traveled and the obstacles encountered along p_i. The exact length of p_i can be easily determined due to an implementational side effect of PREDICT, discussed later in Section 3. Attenuation due to obstacles requires the angle of incidence, which cannot be attained without back-tracing. To avoid the added cost of back-tracing, PREDICT approximates obstacle attenuation of path p_i with a path p where p intersects the centroid of every instantaneous triangular patch whose union defines tetra-wave c. The coefficients of reflection and transmission for path p are computed and stored as c propagates and then used as an approximation of the exact values for path p_i. We chose this approach over back-tracing because experimental evidence showed that the difference between the approximate and exact coefficients was negligible.

2.1.5 Phase and Fast-Fading

As discussed in Section B.3.2, the phase of an incoming path can either add or subtract to the total received power at a query point, causing fast-fading. As one moves a receiving antenna about a close neighborhood to the query point the converging multi-paths will vary in length causing them to move in and out of phase with one another. This phenomena is not modeled by PREDICT because PREDICT is designed as tool for average signal-strength prediction. So in equation 13, the $e^{j(2\pi d(i)/\lambda+\sum f(k))}$ term is dropped. This means that PREDICT's signal prediction is an optimistic measure of the average signal strength at a query point. Note that these equations can be readily altered to account for the phase.

2.1.6 Some Potential Problems in PREDICT's Model

PREDICT and many other prediction systems ignore polarization which may lead to the calculation of unacceptably inaccurate reflection coefficients. Consider Figure 10 which depicts Γ and T across all angles of incidence for perpendicular and parallel polarization. The coefficients for transmission in either the perpendicular or parallel polarization case are about the same, but this is not the case for the coefficients of reflection and, therefore, gross errors may result. For example, if the electric field vector of an incident ray forms a 45 degree angle with the plane of incidence the resulting reflected electric field strength would be a vector sum of the perpendicular and parallel components. Consequently, the average of the two coefficient values would be chosen as the best approximation for Γ rather than choosing either the perpendicular or parallel component, as PREDICT and other systems currently do. Figure 10 plots the average between all such cases.

Another potential source of error when computing reflection and transmission coefficients are the estimated dielectric coefficients for the materials involved. Figure 11 plots the sensitivity of Γ to the dielectric value for the perpendicular and parallel equations for dielectric values 2, 4, 6, 8 and 10. From the graph, for dielectric constants in the range of 4-10, the values for Γ are relatively stable. Since most building materials have dielectric constants in the range of 4-10, one can conclude that exact dielectric constants may not be necessary for reasonable reflection coefficient estimation. Though not shown, similar results occurred for T.

2.2 Amitay's Canyon Model

Amitay's model assumes that the transmitter is positioned in a canyon whose walls are parallel to one another and extend higher than the transmitter's antenna height. Amitay shows in [2] that 10 rays suffice for predicting signal strength when compared to real world measurements. The 10 rays computed are: 1 LOS, 1 ground reflection (GR), 2 single wall reflection (SW), 2 double wall reflection (DW), 2 triple wall reflection (TW) and 2 ground-wall reflection (GW) paths (see figure 3). Since the

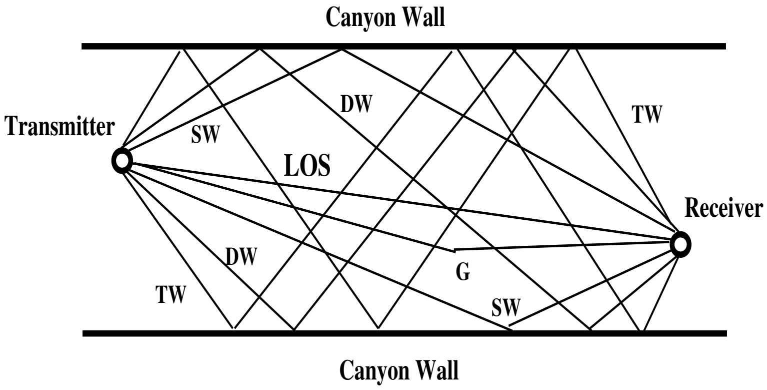

Figure 3: Eight of the ten rays modeled by CANYON

canyon walls are parallel one can devise equations that can exactly compute the path lengths for each of the 10 ray paths for any transmitter and receiver location.

Comparison between the CANYON system and PREDICT in the ideal canyon environment can be found in Section 4. To properly compare the two models, the modeling assumptions and equations used in the CANYON system are identical to those used in PREDICT.

3 PREDICT's algorithm

The PREDICT system maintains the invariant, *when a tetra-wave c captures a query point q that there must exist a path from the transmitter to q which lies completely within the volume swept by c*, while propagating tetra-waves and checking for query point capture efficiently. PREDICT uses a constrained Delaunay triangulation of the environment as the underlying data structure, enabling the implementation of efficient and robust algorithms for tetra-wave propagation and tetra-wave query point capture testing.

The structure of PREDICT's ray-modeling algorithm follows:

* construct the constrained Delaunay triangulation of the terrain and obstacles
* for each transmitter t that exists in the user specified environment:
  -create the initial set of tetra-waves and store them in the *ray-stack*
  -while (ray-stack is not empty)
      * pop the top tetra-wave from the stack
      * propagate the tetra-wave through the environment until an event occurs
      * process the event
      * test for query point capture, updating signal strengths as needed
  -save results

A triangulation [21] is a graph embedded in the plane so that all bounded regions are triangles and so that the unbounded region has convex complement. Any set of planar points P and line segments joining points in P that intersect only at endpoints, *permissible edges*, can be triangulated without adding points. A Delaunay triangulation has the property that the circumcircle of every triangle has empty interior. A set of planar points in general position has a unique Delaunay triangulation. A constrained Delaunay triangulation is a Delaunay triangulation of a planar point set, P, given a forced set of permissible edges E. Such a triangulation has the advantage of producing few extremely small or extremely thin triangles, triangles that could contribute to floating point errors. Note, however, that it is not unique since vertices may have to be added to satisfy the empty circle property.

The set D of points and edges to be triangulated includes the projections onto the xy-plane of the height-field points that describe the contour of the terrain and of the wall edges. If the terrain is flat, no height-field points are included. Shewchuck's TRIANGLE package [24] produces the constrained Delaunay triangulation T of D. The two basic operations on the triangulation are *point location* and *walking*. PREDICT uses the randomized algorithm described in [18]: given a Delaunay triangulation on n vertices and a query point q, determine the location of q with expected cost of $O(\sqrt[3]{n})$. Although theoretically slower than several deterministic algorithms that have a provable $O(\log n)$ query cost ([12], [22], [6]), the randomized algorithm is simple to implement, robust, and efficient in practice. *Walking the triangulation* is the operation that, when given a line segment pq and the triangle containing p, returns all edges of the triangulation that intersect pq as well as the triangle containing q. The walk requires time linear in the number of reported edges. Walking a Delaunay triangulation from p to q has proven efficient in the average case [18].

David Dobkin [5] provided recursive code for the triangulation (tessellation) of the sphere. The starting point is a regular icosahedron, a polyhedron with 20 regular triangular faces and 12 vertices. On each successive recursive step, all triangular faces are subdivided into four new regular triangles. The center of the final tessellated sphere is aligned with the transmitter's location. Let this triangulation be called S.

We construct tetra-waves by defining four rays for each $t \in S$: three of the rays are directed from the center of the tessellated sphere through the three vertices of t; a fourth ray is launched from the center through the centroid p of triangle t. This fourth ray will track the approximate signal power for query point signal-strength calculation. All initial and subsequent tetra-waves are stored in a stack, termed the *ray-stack*.

The test for tetra-wave capture of a query point uses the underlying triangulation. An array indexed on triangle ID stores the list of query points contained by that triangle. Each triangle visited during the propagation of a tetra-wave is stored in a queue. Upon termination of the tetra-wave, the queue of visited triangles selects a subset of query points to be checked for capture.

The processing of a tetra-wave c involves the propagation of c through the environment, which is performed by walking c through the triangulation T. It is important to note that while T appears to lie on the xy-plane, each triangle $t \in T$ actually rep-

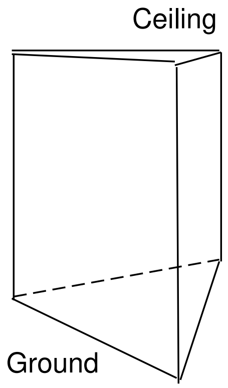

Figure 4: Prism of a triangle of T

resents a 3-dimensional prism (see figure 4): the bottom of the prism is the ground; the top the ceiling; the sides of the prism are vertical and defined by the edges of t. When the terrain is flat, the ground face of a prism will be parallel to the ceiling face; in uneven terrain, the ground face is slanted to match the terrain's contour. The following invariant is maintained: *A tetra-wave c that intersects the prism ρ associated with a triangle $t \in T$ must intersect precisely two of the faces of ρ.*

When a tetra-wave is incident upon a face F of an obstacle, angles of reflection and transmission must be calculated. Each tetra-wave keeps track of a virtual transmitter, initially the actual transmitter. Each of the tetra-wave's rays are reflected to produce the resulting reflected tetra-wave. Let,

c	current tetra-wave
v	c's virtual transmitter
P	plane containing the face F
r_k	r_1, r_2, r_3 define c; r_4 contains its centroid.
p_k	point of intersection between r_k and P

To compute the reflected cone c, first compute the reflections of each r_k by calculating the virtual image $\hat{v}$, of v in P (see Figure 5) and then using $\hat{v}$ to calculate the reflections of rays r_{1-4}. Update tetra-wave c to represent the reflected rays and the new virtual transmitter location $\hat{v}$. The calculation of transmitting rays considers each r_k's angle of incidence and applies Snell's Law of transmission.

The propagation of a tetra-wave may involve any of the following events:

1. Intersection with a wall: As c progresses T, each edge crossed represents either an internal edge or an obstacle wall. If a wall, then 1 (outdoor) or 2 (indoor) new tetra-waves will be created to represent reflected and transmitted components. Push the new rays on the ray-stack.
2. tetra-wave violates invariant: This condition can be identified in constant time: find a face f_k of the prism intersected by the tetra-wave c_i; test each ray r_k of the tetra-wave to see if r_k's intersection point p_{ik} with the plane F_i defined

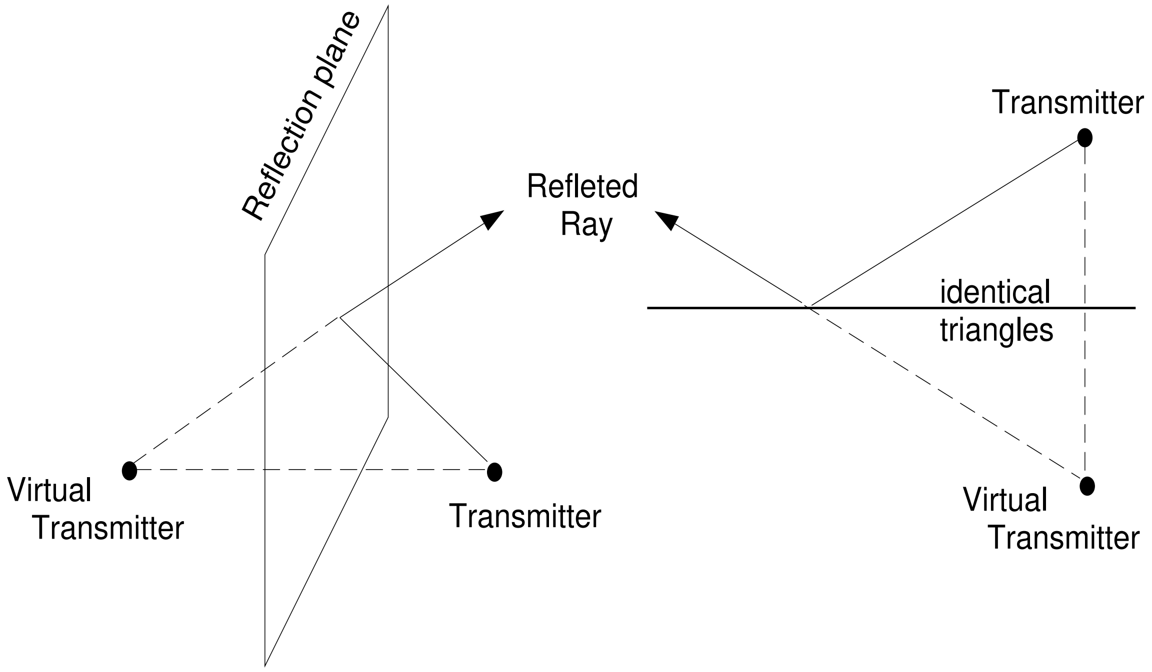

Figure 5: Virtual transmitter (a) skewed side view (b) top view

by f_i lies internal to f_i for $k = 1 - 3$. If any test is negative, c must be split into three or more new tetra-waves (see Figure 6). Recursively test each new tetra-wave for invariant violation. The final output may be as many as fifteen new tetra-waves.

3. Intersection with the ground: reflection based upon a flat plane or upon the three terrain field coordinates of the current triangle $t \in T$
4. Intersection with the ceiling: only active when indoors
5. The tetra-wave's end face area is greater than threshold A: A tetra-wave expands as it propagates. As the tetra-wave expands the approximation of all paths within c by the centroid becomes less accurate. To constrain the error between the approximate path and an arbitrary path in c the tetra-wave will need to be split when c becomes too large. The test to determine whether or not a tetra-wave c must be split depends upon the area of the end triangular face as c traverses T. When c's endface area is too large the tetra-wave c is split into four new tetra-waves according to the template provided by the triangular endface. Midpoints are computed and connected, generating four new tetra-waves.
6. tetra-wave power is below threshold β: Pruning signals whose power is too low to contribute more than a negligible amount to any query point reached improves the efficiency of prediction, as noted by Fortune, *et al.* [7] and Seidel and Rappaport [23]. tetra-waves whose power falls below β, a user definable

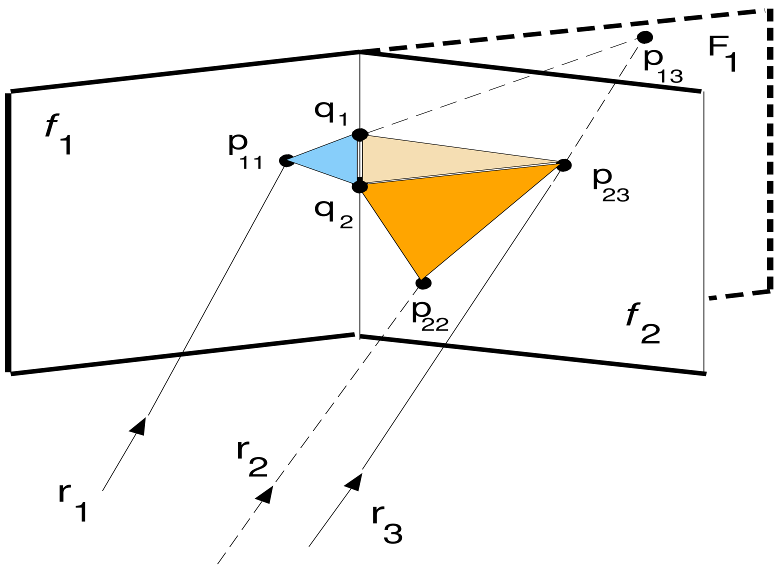

Figure 6: When a tetra-wave intersects more than 3 walls of a prism it must be split into 3 new tetra-waves. The shaded triangles define the new ray cones.

threshold, are processed and discarded.

7. tetra-wave has propagated outside the bounding region: A tetra-wave that walks beyond the boundary of T or propagates above the ceiling in an urban setting has left the boundaries of the environment: it can be processed and discarded.

Diffraction is a distinct event handled separately. When a tetra-wave intersects a wall or terrain edge, diffraction occurs. PREDICT models diffraction as if a transmitter were located at the midpoint of the segment s, defined by the intersection between the tetra-wave and the edge. A wavefront sphere is placed about the new transmitter location and tessellated. tetra-waves are then initialized based upon this new transmitter and tessellated sphere. The code described in Section B.2.4 is then used to define signal power for each newly initialized tetra-wave which are then added to the ray-stack.

As a tetra-wave c propagates through T each triangle traversed by c is stored in a construct X until one of the 1-7 events occurs. Set X is used to construct Q, the set of query points that will be checked for tetra-wave capture where a query point q is in Q iff there exists a $t \in X$ that contains the 2D projection q. Tetra-wave capture involves the construction of a 3-dimensional trapezoid tr constructed from the three defining vectors of the current tetra-wave. Furthermore, the normal vector for each face of tr is pointed inward, which allows for a quick inside of tr test to be performed on each $q \in Q$.

3.1 Corrections for Floating Point Problems

The above describes the case where one uses exact arithmetic. In the case where floating point is used, as in PREDICT, round-off errors can occur that will cause adjacent tetra-waves to become separate or overlapping. In the first case query points may be missed while in the second case a query point q, may be captured twice when q should have only been captured once. The solution to the first problem used by PREDICT is to increase the size of tr, the capture trapezoid, by a value e where e is an estimated upper bound on the maximum occurring separation distance between two adjacent tetra-waves. The value of e is based upon the propagation distance and the number of reflections/transmissions along a tetra-wave path. To solve the second problem PREDICT stores the path of a tetra-wave c and the obstacle ID causing each reflection, transmission and diffraction. This path is unique and thus can be used to determine if more than one tetra-wave with an identical path has captured a query point.

3.2 Potential problems and drawbacks

A problem may occur with terrain height fields that describe cliffs. As discussed in [10] and [15], this can lead to problems due to the creation of long, thin triangles which will reduce the robustness of PREDICT. This problem is not addressed because most cities are not located in extreme terrain.

A drawback to our approach occurs when one applies diffraction in a hilly terrain. The height field will be dense and therefore contain many edges which will be diffracted across, a costly operation.

4 Test Results

The following tests are mainly to show PREDICT's speed and versatility, with the comparison to Amitay's CANYON model as the first step towards validation of PREDICT's prediction accuracy. Overall, the tests cover three environments: an ideal canyon, an urban city on flat terrain and an urban city on a hill. In all three domains transmitters transmit at 950 MHz at a power level of 34mw. All point locations are given in meters and all walls are assumed to be made of brick ($\varepsilon_r = 4.54$). The machine used was a Silicon Graphics Indigo 2 with an SGI IRIX 5.3 operating system. Note that PREDICT provides graphical output for display in GEOMVIEW, a package provide by the Geometry Center at the University of Minnesota.

The canyon is 20 meters wide, 500 meters long and 20 meters high. The transmitter is located at position (1, 5, 5). There are 450 query points in a line where points are spaced one meter apart starting at (50, 4, 2) and ending at (500, 4, 2).

Before applying PREDICT to the canyon domain, two system parameters, the tetra-wave power pruning threshold β and the tetra-wave area splitting threshold

β	-70 dBm	-80 dBm	-85 dBm	-87.5 dBM	-90 dBm
tetra-waves created	5046	20951	39550	52445	64821
Average Difference		6.145	0.731	0.004	0

Table 3: Sensitivity analysis for the β threshold: $A = 5$, maximum number of reflections or transmissions is 3

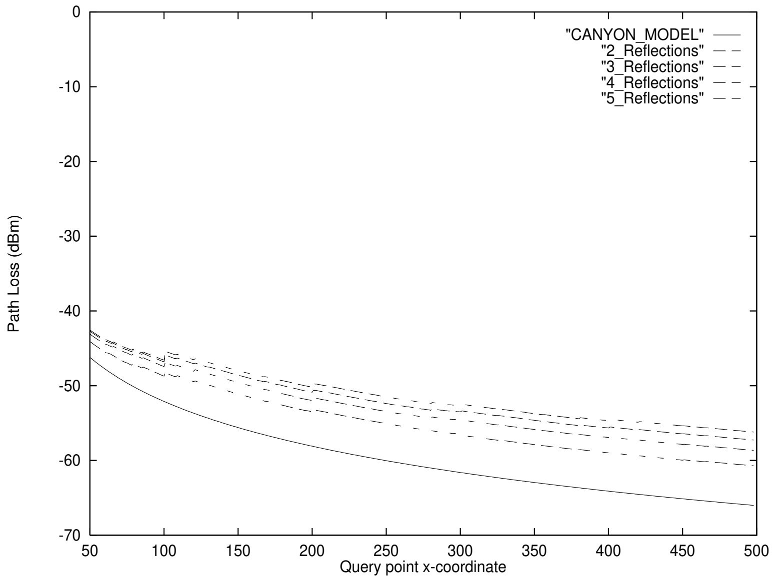

Figure 7: Signal strength predictions for the canyon domain with CANYON and PREDICT where PREDICT is run at 2, 3, 4 and 5 allowed reflections

A, need to be determined. A sensitivity analysis for each parameter was performed where the maximum number of reflections was set at three. Let P be the set of signal strength pairs where pair values (v_1, v_2) are based on predictions made with two different threshold values $parm_1$ and $parm_2$, respectively. A sensitivity difference measure computes the average difference between the pairs of P. Table 3 shows the sensitivity analysis for the β threshold where $parm_1$ and $parm_2$ are two consecutive threshold values. Notice that for threshold values -87.5 and -90 the average difference between predictions is 0. Therefore setting $\beta = -87.5$ should allow for the fastest execution at no loss to predictive accuracy. In similar tests it was determined that $A = 10$ is a good setting. For the rest of the tests $\beta = -87.5$ and $A = 10$, unless stated otherwise.

The comparison of signal strength predictions between PREDICT and CANYON can be found in Figure 7. PREDICT was executed four times with the maximum number of allowed reflections set at 2, 3, 4 and 5, respectively. Not surprisingly, PREDICT's predictions are all slightly higher than CANYON's. The reason for this is that even at the threshold of at most 2 reflections there exist 10 ray paths per

No Splitting	tetra-waves	Triangles Walked	Aver. Walk	Time (min:sec)
Trans (221,701,12)	51690	124593	2.410	
Trans (441,201,8)	27084	55033	2.032	4:13
Splitting				
Trans (221,701,12)	149725	428184	2.860	
Trans (441,201,8)	81390	203608	2.502	12:23

Table 4: Test results for the flat city domain: time is the total for both transmitters

No Splitting	tetra-waves	Triangles Walked	Aver. Walk	Time (min:sec)
Trans (221,701,12)	192392	1009130	5.245	
Trans (441,201,15)	139770	601477	4.303	20:37
Splitting				
Trans (221,701,12)	257401	1382110	6.646	
Trans (441,201,15)	173982	822628	4.728	32:41

Table 5: Test results for the hill city domain: time is the total for both transmitters

query point[3] where two of the signal paths, the two wall-ground paths, are stronger in signal strength than CANYON's two triple-wall signal paths. The test results are positive and also show that Amitay's CANYON model may need to track more than the 10 rays used. Based upon the results and the above discussion, the maximum number of allowed reflections/transmissions will be set at three for the rest of the tests.

The next set of tests demonstrate PREDICT executing in an urban environment. The domain is 600 meters by 800 meters and contains 45 buildings, each with 4 vertical walls. In the first domain the terrain is flat with 220 walls. A hill, whose maximum height reaches 10 meters at (300, 400), is added to the flat city map to create the second domain where the number of height field points describing the terrain is 1444. The second domain contains 2,950 walls, since each triangle face can now be considered a 'wall' of the environment. Figures 12 and 14 depict the two domains with their underlying triangulations. In the flat domain there are two transmitters located at (221,701,12) and (441,201,8). In the hill domain the transmitters are located at (221,701,12) and (441,201,15).

Two tests were executed on each domain: *without* tetra-wave splitting and *with* tetra-wave splitting where Tables 4 and 5 show the number of tetra-waves created, the

[3]at 3 reflections there are 18 ray paths per query point

number of triangles walked, the average number of triangles walked per tetra-wave and the total execution time (note: splitting/no splitting only refers to the user option for event 5, not event 2 which maintains the invariant as described in Section 3). In the flat domain the average difference between prediction strengths for no-split vs. split was 2.966 while in the hill domain it was 3.127. The average signal strength difference between the flat domain and the hill domain was 10.577. Figures 13 and 15 depict the coverage maps for each domain based upon the second test. The lighter gray an area is directly correlates to higher predicted signal strengths[4]. Note the difference a small hill can make to the predicted coverage areas.

From the test results we can conclude that tetra-wave splitting is helpful but not essential. This is important since when placing transmitters a system will need to perform signal strength predictions many times for many transmitter locations. By using PREDICT in a fast execution setting (ie. no splitting), one could speed initial optimization steps substantially. A second conclusion is that terrain, even slight up or down gradients, can greatly affect signal strength prediction. This is a new result that deserves further investigation.

5 Related Work

Several signal strength prediction systems have been created by others. Irrespective of differences based on whether the system does or does not model diffraction and/or scattering, the systems all fall into three categories:

(A) exact path computed by ray-tracing: computationally expensive.
(B) approximate paths computed with forward ray-tracing: efficient but inaccurate.
(C) radio wavefront propagation: faster than (A); more accurate than (B);

PREDICT is a category C system modeled after WISE [8], the first category C system. WISE, which was developed at AT& T, is a fast and robust system that has been combined with a global optimizer and used effectively to determine good or even optimal base-station placements with a computer (see Fortune, *et al.* [9], [27]). Both systems use an underlying triangulation of the environment to provide fast answers to queries. PREDICT and WISE differ, however, in how they model the wavefront. WISE models the wavefront by predetermining the walls upon which the wavefront will be reflecting and transmitting. Each reflected or transmitted wavefront is called a *cone*. When a cone c contains ("captures") a query point, WISE computes the actual radio signal path by back-tracing the path based upon the reflections and transmissions undergone by the cone c. Back-tracing is used because the cones can vary dramatically in size, and the signal power variance across a cone could be large. The center of the cone will not be a good approximation to the power of the exact path.

[4]In GEOMVIEW these images are in color

We believe that modeling of the wavefront through tessellation of the wavefront sphere represents an improvement over all category (A) and (B) systems. PREDICT's algorithm is straight forward: walk a tetra-wave until the tetra-wave needs to be split, reflected, transmitted, diffracted or killed. This simplicity allows PREDICT to be robust, efficient and applicable in many environments. Furthermore, due to the similarity between PREDICT and a ray-tracing system, PREDICT can be augmented into parallel system with minimal effort. In WISE, identification of walls, subsections of walls (due to shadowing) and floor/ceiling polygonal sections must all be computed for the system to know which wavefront to reflect, transmit and diffract. Due to this added algorithmic complexity, WISE currently does not support varied terrain and is not easily modified to work in parallel. Last, PREDICT is freely available for research while WISE is only available through AT& T.

6 Future Work

A clear next step is to compare PREDICT's signal prediction with real world data. This would provide an essential step towards validation of PREDICT's model.

Currently PREDICT cannot model multiple floors of a building. This is a problem since between floor ducts and between floor interference cannot be modeled. By using a method from [8] and [7] PREDICT can be extended for multi-floor modeling. The method involves treating each floor (or duct space) as a single environment. Recall that an environment has an associated triangulation. tetra-waves propagate in their current environment E, until a floor or ceiling intersection occurs. At this point the system uses point location to locate the tetra-wave in E_f or E_c, the environments that lie below or above E, respectively. Once located in the new environment's triangulation, tetra-wave propagation prediction is continued as usual.

Omni-directional antennas are the only antenna types supported by PREDICT. Extension of PREDICT to provide a means of defining the power output for directed antennas would be useful.

Walls of buildings, inside or out, often have extra features like windows and doors. PREDICT should be extended to allow walls to contain convex shapes with their own associated electrical properties. A quick check would allow a tetra-wave to reflect off of these varied features and provide better predictive accuracy.

7 Conclusion

PREDICT is a general radio wave propagation engine whose algorithms are robust and applicable across all current environments of interest. PREDICT's model is based upon current field tested ray-tracing models which have proven to be accurate. The system has been designed to provide radio signal prediction for wireless network engines and as a research tool for researcher's wishing to validate their own modeling methods. In both of these areas PREDICT should prove useful due to its speed, flexibility and simplicity of design.

References

[1] S. A. Abbas and A. U. H. Sheikh. Narrow-band small area microcellular mobile radio channel characterization using ray tracing technique. In *IEEE 43rd Vehicular Technology Conference*, pages 589–592, 1993.

[2] Noach Amitay. Modeling and computer simulation of wave propagation in lineal line-of-sight microcells. *IEEE Transactions on Vehicular Technology*, 41(4):337–342, 1992.

[3] C. A. Balanis. *ANTENNA THEORY: Analysis and Design.* Harper and Row, New York, 1982.

[4] C. A. Balanis. *Advanced Engineering Electromagnetics.* John Wiley and Sons, New York, 1989.

[5] D. P. Dobkin. Tesselation of a sphere. Technical report, Princeton University, 1997.

[6] H. Edelsbrunner, L. J. Guibas, and J. Stolfi. Optimal point location in a monotone subdivision. *SIAM J. Comput.*, 15:317–340, 1986.

[7] S. J. Fortune. Algorithms for prediction of indoor radio propagation. Technical Report an internal report, Bell Atlantic a subsidiary of Lucent Technologies, 1996.

[8] S. J. Fortune. A beam-tracing algorithm for prediction of indoor radio propagation. In *Lecture Notes in Computer Science V,1148: Applied computational geometry: towards geometric engineering*, 1996.

[9] S. J. Fortune, D. M. Gay, B. W. Kernighan, O. Landron, R. A. Valenzuela, and M. H. Wright. Wise design of indoor wireless systems: practical computation and optimization. *IEEE Computational Science and Engineering*, pages 58–68, 1995.

[10] M. Garland and P.S. Heckbert. Fast polygonal aproximation of terrains and height fields. Technical Report to appear, Carnegie-Mellon, 1996.

[11] U. B. Halabe, A. Sotoodehnia, K. R. Maser, and E. A. Kausel. modeling the electromagnetic properties of concrete. *ACI Materials Journal*, 90(6):552–563, 1993.

[12] D. G. Kirkpatrick. Optimal search in planar subdivisions. *SIAM J. Comput.*, 12(1):28–35, 1983.

[13] R. G. Kouyoumjian and P. H. Pathak. A uniform geometrical theory of diffraction for an edge in a perfectly conduction surface. *Proceedings IEEE*, 62(11):1448–1461, Nov. 1974.

[14] P. Kreuzgruber, T. Brundl, W. Kuran, and R. Gahleitner. Prediction of indoor radio propagation with the ray-splitting model including edge diffraction and rough surfaces. In *Proceedings of the 1994 IEEE 44th Vehicular Technology Conference*, pages 878–882, 1994.

[15] Marc Van Kreveld. Digital elevation model: overview and selected tin algorithms. Technical Report to appear, Utrecht University, 1996.

[16] D. I. Laurenson, S. McLaughin, and A. U. H. Sheikh. The application of ray tracing and the geometrical theory of diffraction to indoor channel modelling. In *IEEE Global Telecommunications Conference*, pages 1242–1246, 1993.

[17] G. Lombardi, V. Degli-Esposti, C. Passerini, G. Riva, and E. Valentinuzzi. Measurement and simulation of the dect indoor propagation channel. In *1997 IEEE Vehicular Technology Conference (VTC '97)*, pages 426–430, Phoenix, AZ, May 1997.

[18] E. Mucke, I. Saias, and B. Zhu. Fast randomized point location without preprocessing in two and three-dimensional delaunay triangulations. In *Proc. of the 12th Annual Symp. on Computational Geometry*, pages 274–283, 1996.

[19] Short Course Notes. The modern geometrical theory of diffraction. Technical report, ElectroScience Lab., Ohio State University, 1996.

[20] J. D. Parsons. *The Mobile Radio Propagation Channel*. Wiley and Sons, New York, 1992.

[21] F. P. Preparata and M. I. Shamos. *Computational Geometry*. Springer Verlag, New York, 1985.

[22] N. Sarnak and R.E. Tarjan. Planar point location using persistent search trees. *Communications of the ACM*, 29(7):669–679, 1986.

[23] S. Y. Seidel and T. S. Rappaport. Site-specific propagation prediction for wireless in-building personal communication system design. *IEEE Transactions on Vehicular Technology*, 43(4):879–891, Nov. 1994.

[24] J. Shewchuck. Triangle: Engineering a 2d quality mesh generator and delaunay triangulator. In *First ACM workshop on Applied Computational Geometry*, pages 124–134, 1996.

[25] R.R. Skidmore, T.S. Rappaport, and A.L. Abbott. Interactive coverage region and system design simulation for wireless communication systems in multifloored indoor environments: Smt plus in multifloored indoor environments. In *ICUPC 96*, Boston, MA, 1994.

[26] C. K. Sou, O. Landron, and M. J. Feuerstein. Characterization of electromagnetic properties of building materials for use in site-specific propagation prediction. Technical Report MPRG-TR-92-12, Virginia-Tech, 1992.

[27] Fernando J. Velez and Jose M. Brazio. A computational-geometry-based tool for the cellular design of millimetrewave mobile communication systems in urban environments. In *First CGC workshop for Computational Geometry*, 1996.

A Terminology

Environments are typically characterized as rural, suburban, urban and in-building. Transmitters are also characterized by the size of the areas they are to cover: large areas are termed macrocells; medium-sized areas, microcells; and small areas, picocells. Typically, macrocell transmitters are used in rural and suburban areas, microcell transmitters in suburban and urban areas and picocell transmitters for in-building coverage.

B Radio Background

The following provides a brief overview of electromagnetic wave theory and the modeling of radio signals with geometric optics with respect to the issues concerning the modeling and propagation of radio waves. For additional information, some good references are [4], [3] and [20].

B.1 Radio Wave Propagation Theory

A radio signal is an electromagnetic wave whose behavior can be characterized using Maxwell's equations which describe the time varying behavior of an electromagnetic field. Even approximate solutions of Maxwell's equations are extremely costly and thus impractical in large instances. The strategy for modeling the propagation of radio waves used in this paper comes from the field of geometric optics (GO) where the radio signal, an electromagnetic wave, is modeled by a ray. A ray is defined by an initial starting point and a directed vector. In this model, the initial starting point is the transmitter while the directed vector defines the radio signal's direction of propagation and the distance traveled with respect to time t.

The GO model treats radio signal propagation as if the radio wave were a particle. Therefore, in this modeling scheme, it is important to recognize when the model needs to be extended to properly characterize the wave characteristics of the electromagnetic field.

Section B.2 provides an overview of the issues involved when modeling a radio signal with a ray. Section B.3 describes how the signal strength at a received point can be computed with respect to the ray model (or GO model).

B.2 GO Modeling Overview

As a radio signal propagates through the environment it will encounter various obstacles where reflection, transmission, scattering and diffraction of the radio signal will occur. Attenuation, a decline in the strength of the electromagnetic field, occurs as the radio signal propagates and encounters obstacles. The amount of attenuation is determined by the radio wave's frequency and the electrical properties of the matter the radio wave travels through. Each of these modeling issues will now be discussed. The variables f, c, λ and P are defined as follows:

f	frequency
c	speed of light (3×10^8 m/s)
$\lambda = c/f$	wavelength
P	radio signal's power

Given a volume of a specific type of matter, it is convenient to assume that throughout the volume the matter is uniform in density and electrical properties. An ideal volume of matter that a radio signal is propagating through is termed the *medium* of propagation.

B.2.1 Electrical Properties of Matter

The electrical properties of a volume of matter under the influence of a static or traveling electromagnetic field can be characterized by three constants: the dielectric constant, the relative permeability and the conductivity of the material in question. Attaining accurate values for these constants is non-trivial and represents an area of ongoing research.

$\varepsilon_r = \varepsilon_s/\varepsilon_0$	dielectric constant (relative permittivity)
$\mu_{rs} = \mu_s/\mu_0$	relative permeability
σ_s	conductivity

where

ε_0	free space permittivity
μ_0	free space permeability

ε_s	material's permittivity
μ_s	material's permeability

These values, ε_r, μ_{rs} and σ_s roughly define the materials ability to store a charge, the amount of magnetic polarization that occurs when subjected to a magnetic field and its ability to carry an electric current, respectively. The constants ε_0, μ_0, ε_s and μ_s must be measured with respect to the applied electromagnetic field since the frequency and type, static or traveling, of the applied electromagnetic field affects the resulting values. Note that it is common practice to use the square root of the dielectric constant as the material's index of refraction.

A radio signal exerts a traveling electromagnetic field upon a material. As discussed above, the dielectric, permeability and conductivity constants depend upon the frequency of the radio signal and the physical characteristics of the obstacles. The simulation of radio propagation is impeded by the fact that one often does not know exactly what types of materials have gone into the construction of a wall or building. Currently, site-specific measurements must be taken to attain accurate values for these constants. Current research focuses on determining functions that effectively approximate these values. Halabe *et al.* propose a method for approximating concrete dielectric properties in [11].

B.2.2 Signal Attenuation

As an electromagnetic wave propagates through a medium the field loses energy due to current conduction and dissipation in the form of heat. This loss of energy is defined as signal attenuation, α, and is a constant for a specific type of medium and signal frequency. The conductivity of a medium is the most important factor since conductive materials exert a strong influence upon the electromagnetic field. Good conductors greatly attenuate a signal while good dielectrics (poor conductors) cause only slight signal attenuation.

$$\alpha = \omega\sqrt{\mu\varepsilon}\left[\frac{1}{2}\left(\sqrt{1+\left(\frac{\sigma}{\omega\varepsilon}\right)^2}-1\right)\right]^{\frac{1}{2}} \qquad Np/m \tag{1}$$

where

$$\omega = 2\pi f \qquad rad/s$$

A simplification can be made by classifying the medium as either a good dielectric or a good conductor.

	good dielectric $\left(\frac{\sigma}{\omega\varepsilon}\right)^2 \ll 1$	good conductor $\left(\frac{\sigma}{\omega\varepsilon}\right)^2 \gg 1$
α	$\cong \frac{\sigma}{2}\sqrt{\frac{\mu}{\varepsilon}}$	$\cong \sqrt{\frac{\omega\mu\sigma}{2}}$

For example, if air is the medium then $\varepsilon = 1.0006$, $\mu \cong 1$, $\sigma \cong 0$ so $\alpha = 0$. When $\alpha \cong 0$ the medium is termed lossless, as opposed to lossy where $\alpha > 0$. When a medium is lossless the type of signal attenuation just described can be ignored. Air, brick and dry soil are all examples of lossless mediums since these materials are all poor conductors. Note that one may wish to calculate attenuation for very humid air, damp brick or wet soil since signal attenuation through these mediums may have a measurable impact upon the resulting signal strength.

A radio signal also attenuates because it is part of an ever expanding wavefront. As the wavefront expands the electromagnetic field becomes spread over an ever increasing area. The amount of energy per unit area decreases as the wavefront propagates.

B.2.3 Reflection and Transmission

When a radio signal intersects an obstacle, both reflection and transmission of the electromagnetic wave occur. Under the GO model, the strength of each reflected and transmitted component is determined by computing the reflection and transmission coefficients, Γ and T, which depend upon the two mediums involved and the radio signal's angle of incidence and polarization. The angle of incidence is acute angle formed between the intersection of reflection plane with the plane of incidence, which is defined by the signal's propagation vector and by the normal vector to the reflection plane at its intersection point with the signal (see Figures 8 and 9). The polarization of a radio signal is a vector representing the instantaneous state of the electric field at a given time t where, in this case, t represents the time of intersection. The polarization vector is usually described by its parallel and perpendicular components, where parallel and perpendicular are w.r.t. the plane of incidence. Each component, perpendicular and parallel, must then be handled individually. The final reflected and transmitted field strengths are determined by summing the resulting reflected and transmitted perpendicular and parallel components. Finally, the two mediums involved determine the equations used to calculate Γ and T for each perpendicular and parallel field case. Each of these factors is discussed in greater detail below.

Normally, the radio signal will travel some distance through air, a good dielectric, before encountering an obstacle. The second medium, the obstacle, might be anything from a wall of a building, a car or a person and, consequently, the second medium may be a good dielectric, a good conductor or a semiconductor. The two cases, dielectric-dielectric and dielectric-conductor, must be addressed. The case where one has a dielectric-semiconductor[5] interface must be approximated by the dielectric-dielectric case with signal attenuation (recall that semiconductors and conductors are lossy materials). The dielectric-conductor case can be simplified with the assumption that if the second medium is a good conductor it will provide total reflection with no transmission (justifying details can be found in [4]). The dielectric-dielectric case is

[5] Some examples of semiconductors are people, glass and seawater.

discussed below, following the discussion on signal polarization.

A radio signal has an associated electric field E. At the time of intersection the incidence of E upon the reflecting plane is defined by E's instantaneous polarization vector v. In practice E and v are separated into two components, the perpendicular and parallel components $E_\perp$, $E_\parallel$, $v_\perp$ and $v_\parallel$, whose vector sums equal E and v respectively, where $E_\perp$ ($E_\parallel$) is the component of the electric field E that is perpendicular (parallel) to the plane of incidence. When one calculates the reflection and transmission coefficients Γ and T, one first calculates $\Gamma_\perp$, $\Gamma_\parallel$, $T_\perp$ and $T_\parallel$, based upon E and v. Γ and T are then computed by taking the vector sum of $\Gamma_\perp$, $\Gamma_\parallel$ and $T_\perp$, $T_\parallel$, respectively. The polarization of an electromagnetic wave can fall into three categories: linear, elliptic and circular.

In the geometric optics model the angles of reflection and transmission adhere to Snell's Laws of reflection and transmission (see Figures 8 and 9). Let,

θ_i, θ_r, θ_t	angle of incidence, reflection and transmission
$E_\perp$, $E_\parallel$	perpendicular and parallel components of E
$H_\perp$, $H_\parallel$	components of H, the magnetic field
$\Gamma_\perp$, $\Gamma_\parallel$	perpendicular and parallel reflection coefficients
$T_\perp$, $T_\parallel$	perpendicular and parallel transmission coefficients
μ_1, ε_1	permeability and dielectric values for medium 1
μ_2, ε_2	permeability and dielectric values for medium 2

where

$\theta_r = \theta_t$	Snell's law of reflection
$\sin\theta_t / \sin\theta_i = i$	Snell's law of refraction
$i \cong \frac{\sqrt{\mu_1/\varepsilon_1}}{\sqrt{\mu_2/\varepsilon_2}}$	index of refraction

For the perpendicular (horizontal or E) polarization in the dielectric-dielectric case we have (see figure 8)

$$\Gamma_\perp = \frac{\cos\theta_i\sqrt{\frac{\mu_2}{\varepsilon_2}} - \cos\theta_t\sqrt{\frac{\mu_1}{\varepsilon_1}}}{\cos\theta_i\sqrt{\frac{\mu_2}{\varepsilon_2}} + \cos\theta_t\sqrt{\frac{\mu_1}{\varepsilon_1}}} \tag{2}$$

$$T_\perp = \frac{2\cos\theta_i\sqrt{\frac{\mu_2}{\varepsilon_2}}}{\cos\theta_i\sqrt{\frac{\mu_2}{\varepsilon_2}} + \cos\theta_t\sqrt{\frac{\mu_1}{\varepsilon_1}}} \tag{3}$$

If $\mu_1 \cong \mu_2 \cong \mu_0$, which is the case for most dielectrics, equations 2 and 3 can be simplified to,

$$\Gamma_\perp = \frac{\cos\theta_i - \sqrt{\frac{\varepsilon_2}{\varepsilon_1}}\sqrt{1 - \left(\frac{\varepsilon_2}{\varepsilon_1}\right)\sin^2\theta_i}}{\cos\theta_i + \sqrt{\frac{\varepsilon_2}{\varepsilon_1}}\sqrt{1 - \left(\frac{\varepsilon_2}{\varepsilon_1}\right)\sin^2\theta_i}} \tag{4}$$

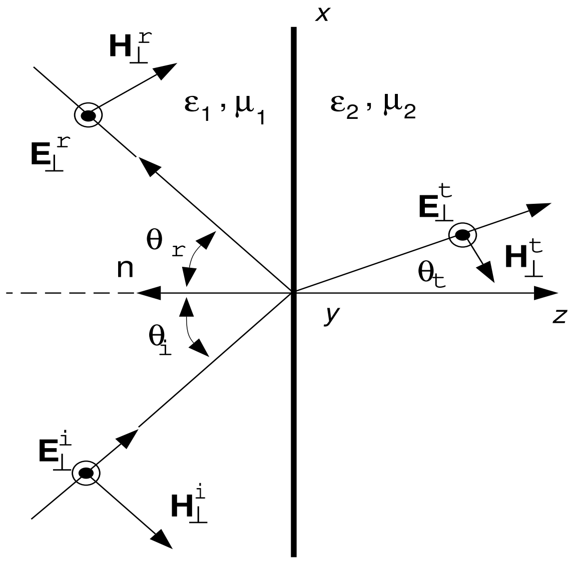

Figure 8: Perpendicular (horizontal) polarized wave incident at an oblique angle to the reflection plane

$$T_\perp = \frac{2\cos\theta_i}{\cos\theta_i + \sqrt{\frac{\varepsilon_2}{\varepsilon_1}}\sqrt{1-\left(\frac{\varepsilon_2}{\varepsilon_1}\right)\sin^2\theta_i}} \tag{5}$$

For the parallel (vertical or H) polarization in the dielectric-dielectric case we have (see figure 9)

$$\Gamma_\parallel = \frac{-\cos\theta_i\sqrt{\frac{\mu_1}{\varepsilon_1}} + \cos\theta_t\sqrt{\frac{\mu_2}{\varepsilon_2}}}{\cos\theta_i\sqrt{\frac{\mu_1}{\varepsilon_1}} + \cos\theta_t\sqrt{\frac{\mu_2}{\varepsilon_2}}} \tag{6}$$

$$T_\parallel = \frac{2\cos\theta_i\sqrt{\frac{\mu_2}{\varepsilon_2}}}{\cos\theta_i\sqrt{\frac{\mu_1}{\varepsilon_1}} + \cos\theta_t\sqrt{\frac{\mu_2}{\varepsilon_2}}} \tag{7}$$

As before, if $\mu_1 \cong \mu_2 \cong \mu_0$, which is the case for most dielectrics, equations 6 and 7 can be simplified to,

$$\Gamma_\parallel = \frac{-\cos\theta_i + \sqrt{\frac{\varepsilon_1}{\varepsilon_2}}\sqrt{1-\left(\frac{\varepsilon_1}{\varepsilon_2}\right)\sin^2\theta_i}}{\cos\theta_i + \sqrt{\frac{\varepsilon_1}{\varepsilon_2}}\sqrt{1-\left(\frac{\varepsilon_1}{\varepsilon_2}\right)\sin^2\theta_i}} \tag{8}$$

$$T_\parallel = \frac{2\cos\theta_i\sqrt{\frac{\varepsilon_1}{\varepsilon_2}}}{\cos\theta_i + \sqrt{\frac{\varepsilon_1}{\varepsilon_2}}\sqrt{1-\left(\frac{\varepsilon_1}{\varepsilon_2}\right)\sin^2\theta_i}} \tag{9}$$

Finally,

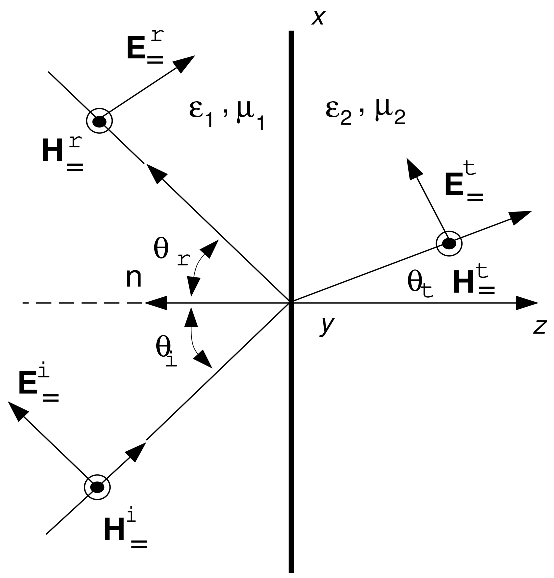

Figure 9: Parallel (vertical) polarized wave incident at an oblique angle to the reflection plane

$$E_r = E_\perp \times \Gamma_\perp + E_\| \times \Gamma_\| \qquad \text{reflected field strength}$$
$$E_t = E_\perp \times T_\perp + E_\| \times T_\| \qquad \text{transmitted field strength}$$

Note that $E_\perp + E_\| = E$ and $|\Gamma_\perp| + |T_\perp| = 1$ since we are dealing with lossless mediums. The above coefficients are often referred to as the *Fresnel reflection and transmission coefficients*. From before, for the dielectric-conductor case $\Gamma_\perp \cong \Gamma_\| \cong 1$. The entire radio signal is reflected. This assumes that the second medium is a good conductor like copper and steel. In the dielectric-semiconductor case one must use the dielectric-dielectric formulas and then attenuate the transmitted component of the signal. The amount of attenuation is determined by α, from Section B.2.2, and the distance traveled within the lossy medium.

Note that when $\varepsilon_2/\varepsilon_1 > 1$ both Γ and T are real, as will always hold in an air-obstacle case. When $\varepsilon_2/\varepsilon_1 < 1$ both Γ and T are real up to an incidence angle $\theta_i = \theta_c$, where both Γ and T become complex. The value θ_c is referred to as the critical angle and represents the angle at which total internal reflection occurs.

The reflected and transmitted signal components may also undergo phase shifts and polarization effects. Discussion of these topics goes beyond the scope of this paper. Suffice it to say that, to model a reflected or transmitted signal through to its final state, phase shifts and polarization effects must be taken into account.

B.2.4 Diffraction and Scattering

Diffraction of the radio signal occurs when the radio wave intersects an obstacle at a corner, an edge formed between two planes (a wedge) or along the tangent to a curved surface. In the geometric optics model, the strength of diffracted radio signals can be computed using the uniform theory of diffraction Kouyoumanjian and Pathak [13]. The model from [13] is extended in [19], where code for computation of the two keller coefficients of diffraction, D_s and D_h, is provided for wedge diffraction. Given the angle of incidence (θ_i), the signal's phase (β), the wedge angle (ϕ), the point of incidence on the wedge and an observation point the code will compute the two coefficients, D_s and D_h. These coefficients can then be used along with the radio signal's electric field vector (v), the instantaneous polarization vector at the time of intersection, to compute the radio signal strength at the observation point. D_s applies to the perpendicular (horizontal) component of v while D_h applies to the parallel (vertical) component of v.

Scattering of a radio signal occurs because the surfaces that reflect, transmit and diffract signals are not ideally smooth. Surfaces have irregularities and these irregularities cause scattering of the radio signal. The amount of scattering that occurs depends upon surface roughness, the angle of incidence and the signal's wavelength, λ.

B.3 Multi-path Signal Strength Computation

In a city or the floor of a building many paths may exist from transmitter to receiver due to reflection, transmission, scattering and diffraction. The sum of all paths from transmitter to receiver determines the signal strength at the receiver, P_r. A single path may add or subtract from the current total depending upon the signal's phase at the receiver.

B.3.1 Computing the power of a propagation path

A propagation path, p, is a path of a single radio signal from the transmitter to receiver. In the geometric optics (GO) model this path is a polygonal chain whose internal vertices lie on obstacles in the environment. Let d be the total length of p from transmitter to receiver. If p is a line-of-sight (LOS) path then the power transmitted over p to the receiver can be computed by using Friis's free space formula ([20]):

$$P_r = P_p * G_r * \left(\frac{1}{d}\right)^2 \tag{10}$$

where P_p is the signal's power 1 meter from the transmitter

$$P_p \cong P_t * G_t * \left(\frac{\lambda}{4\pi}\right)^2 \tag{11}$$

G_t and G_r define the transmitter and receiver *antenna gains* and P_t is the power input to the transmitter's antenna array. An antenna may not create a uniform electromagnetic field, this variation of power output across the wavefront is termed the *antenna gain.* G_t is used to compute the antenna gain for a particular direction centered upon and directed from the transmitter's location. Similarly, a receiver may not be uniformly receptive to all possible incoming radio signals. G_r defines the non-uniform sensitivity for a receiver to incoming signals. When the transmitter and receiver are omni-directional, $G_t = G_r = 1$.

When the path contains one or more reflections or transmissions the coefficients for each reflection and transmission must be calculated and then used to attenuate the signal's power accordingly.

$$P_r = P_p * G_r * \left(\frac{1}{d}\right)^2 * R * T \tag{12}$$

where $R = r_1 * r_2 * ...r_j$ and $T = t_1 * t_2 * ...t_k$ and $r_{1..j}$ $(t_{1..k})$ are all of the calculated reflection (transmission) coefficients for path p.

In the case where p is a path that scatters or diffracts the radio signal, the computation of P_p will need modification. When a radio signal is scattered or diffracted, its electromagnetic field disperses. In effect, the original radio signal is gone; its energy spreads in all directions about the point of intersection. This dispersed field of energy can be thought of as a 'new' transmitter t_n which is emitting a new radio wavefront where gain G_n of t_n can be computed with GO models of scattering and diffraction. Therefore, in the path power calculations, P_p should be the computed power of the signal after the radio signal was scattered or diffracted.

B.3.2 Summing the Multi-Path

Each propagation path either adds to or subtracts from the total sum of power depending upon the signal's phase at the receiver. If p_i represents path i's power at the receiver then

$$P_r = \sum p_i e^{j\left(2\pi d(i)/\lambda + \sum f(k)\right)} \tag{13}$$

where
$d(i)$ is the path length for each p_i
$f(k)$ is the phase shift that occurred when the signal was reflected or transmitted during propagation (either 0 or 180) where $k = 0...\#$ reflections

Note that the complex term in the equation computes the phase for signal p_i. Depending upon the phase, signal p_i may add or subtract from the total received signal power.

B.3.3 Path Loss and Delay Spread

In the radio field, *path-loss* is used as a convienient representation for received signal strength: path-loss $= 10 * \log 10(P_r/P_t)$. An example use is that normally a path loss > -70 dBm is usually necessary for reliable communication. This is convienient since -70 dBm holds for any transmitting power level, P_t.

Let p_s and p_l represent the shortest and longest multi-path components of a received signal. The delay spread at the receiver would be $(d_l - d_s)/c$. The delay spread is a multi-path phenonema measuring the time interval between incoming signals. Signals having a distance $d_i - d_s >$ 300 meters will not add to the computated signal strength but will instead cause interfence.

B.3.4 Average Signal Strength and Fast-Fading

Place a one meter radius sphere, s, about a point, p. The average signal strength for p is the average signal power over s. In practice, field measurements are taken in multiple positions about a location and then averaged. These measurements will take into account multi-path signal phase as well as any co-channel interference and/or background noise that may exist at the time of measurement. Fast fading is the effect of multi-path signal cancellation due to one or more signals being out of phase. Within sphere s the signal strength will fluctuate due to fast-fading effects where the wavelength λ will largely determine the number and severity (smaller will in general increase the number of fluctuations). Both types of signal strength prediction are useful for researchers and network engineers. Currently, most systems only provide average signal strength prediction since how to properly model fast-fading effects is still not well understood (SMT Plus [25] uses statistical models based upon large numbers of field measurements to predict fast-fading effects).

B.3.5 Polarization Loss

A receiving antenna has an associated electric field E with an associated polarization vector v. The polarization of incoming radio signals rarely match polarization v, which causes some signal attenuation termed *polarization loss*. Usually this loss is low, around -3 dBm (see [3]).

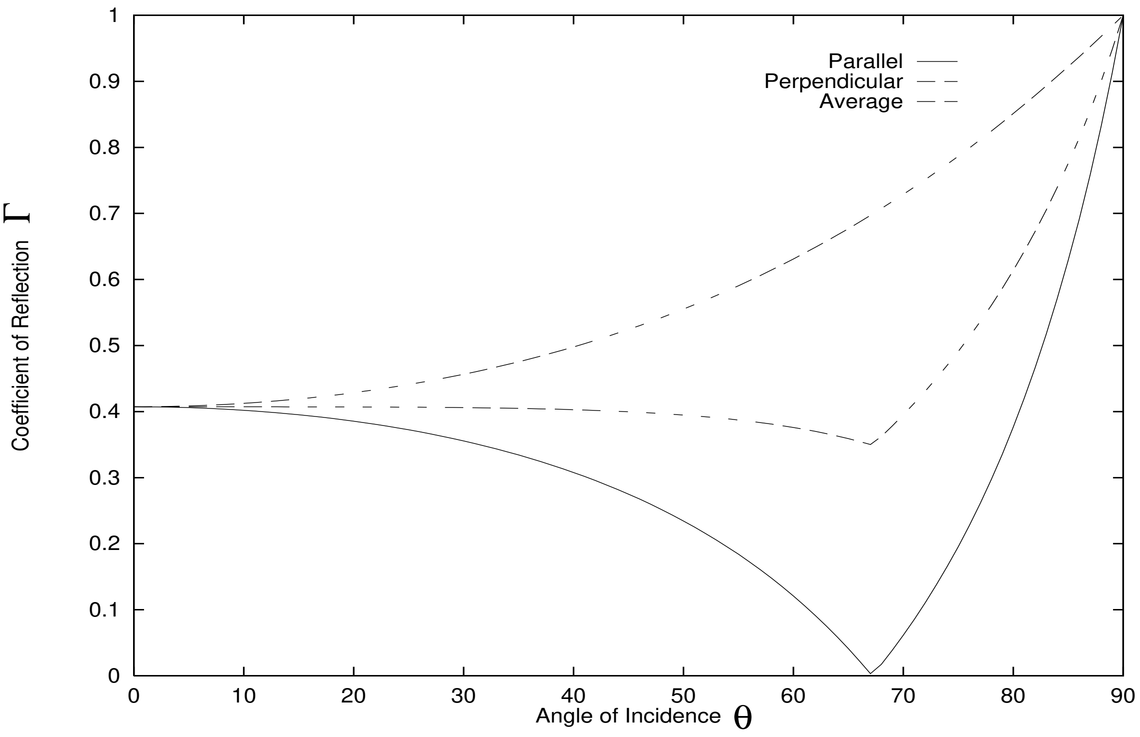

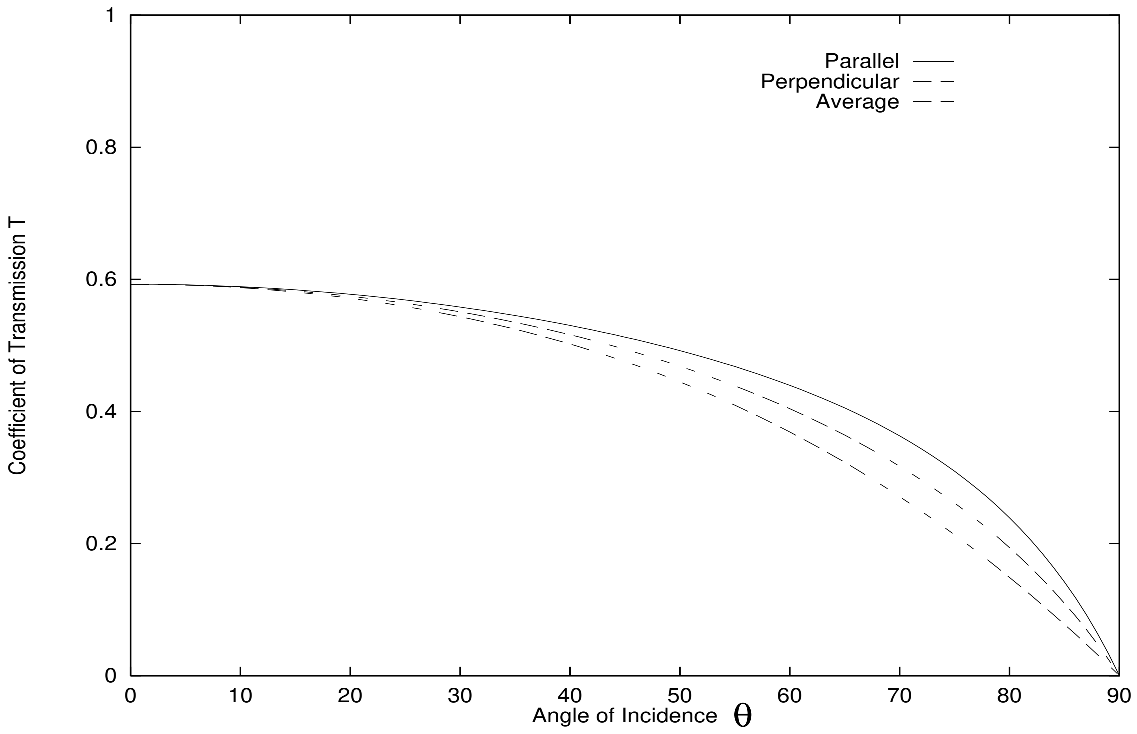

Figure 10: Parallel and Perpendicular coefficient plots for reflection and transmission

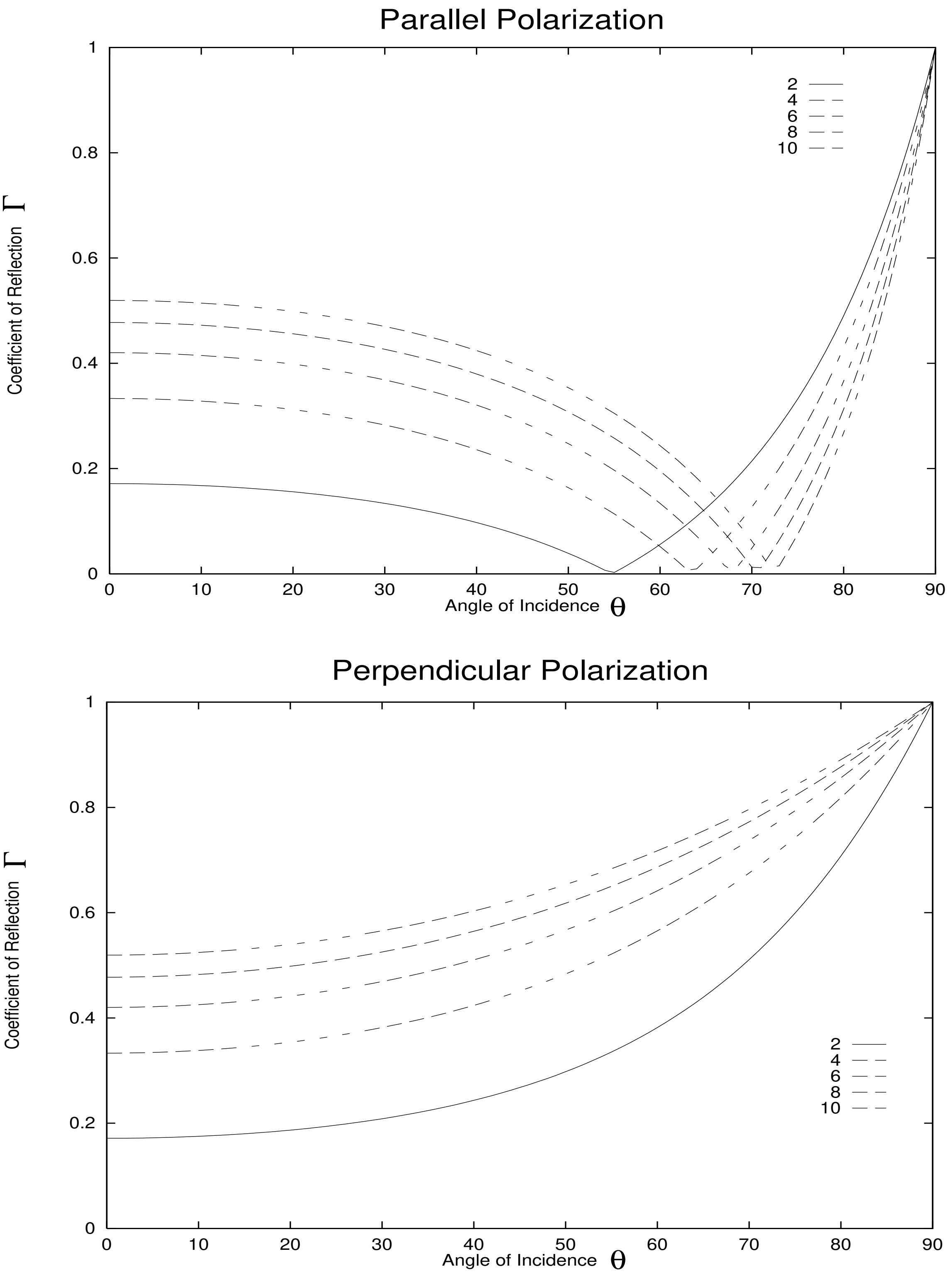

Figure 11: Coefficient of reflection plots for dielectric values ranging from 2-10

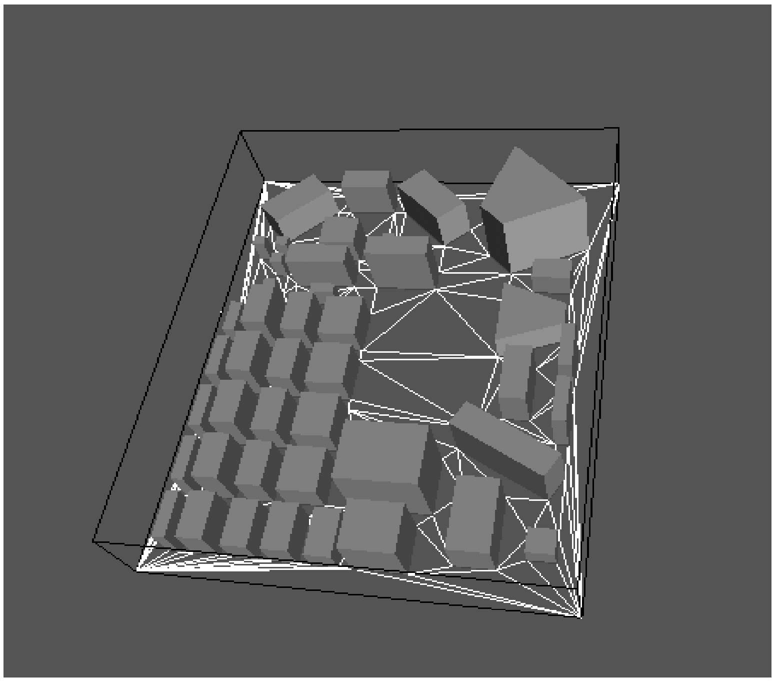

Figure 12: The flat city domain and underlying triangulation

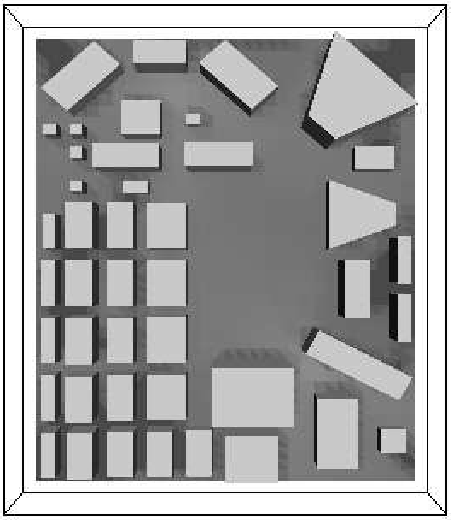

Figure 13: Coverage map for the flat city domain: lighter areas have higher predicted signal strengths

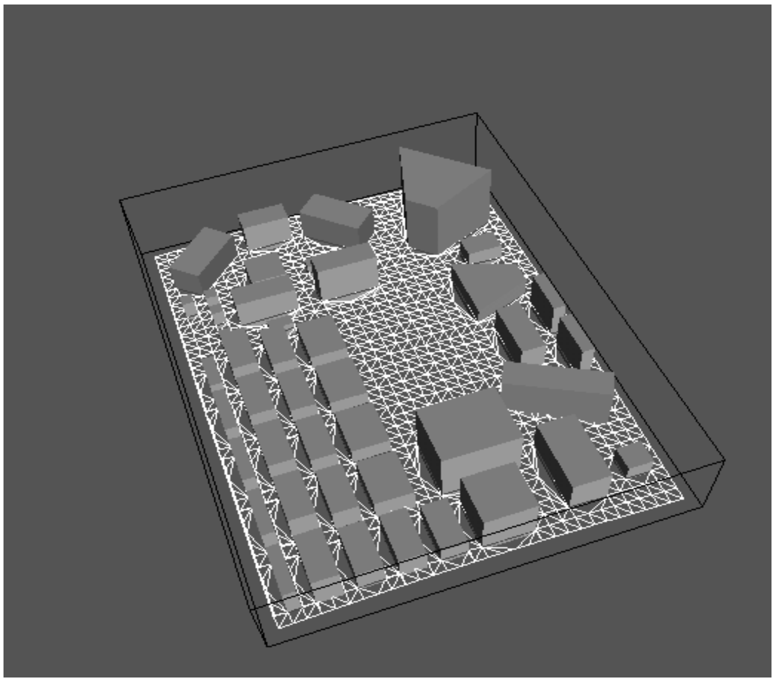

Figure 14: The hill city domain and underlying triangulation

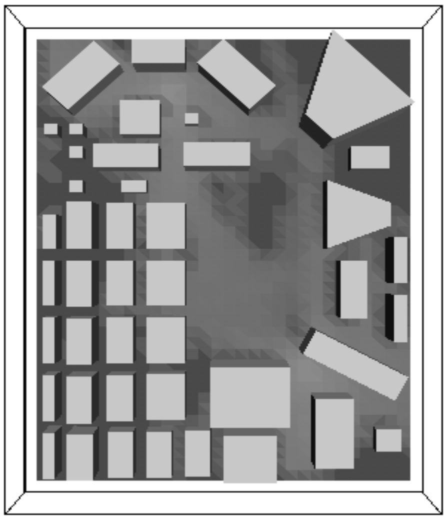

Figure 15: Coverage map for the hill city domain: lighter areas have higher predicted signal strengths